

## Research Article

# Magnetic Circuit Optimization and Physical Modeling of Giant Magnetostrictive Actuator

Yuesong Li <sup>1,2</sup>

<sup>1</sup>School of Mechatronics Engineering, Henan University of Science and Technology, Luoyang 471003, China

<sup>2</sup>Collaborative Innovation Center of Machinery Equipment Advanced Manufacturing of Henan Province, Luoyang 471003, China

Correspondence should be addressed to Yuesong Li; [liyaosong707@163.com](mailto:liyaosong707@163.com)

Received 12 November 2022; Revised 26 April 2023; Accepted 22 May 2023; Published 9 June 2023

Academic Editor: Jin Huang

Copyright © 2023 Yuesong Li. This is an open access article distributed under the Creative Commons Attribution License, which permits unrestricted use, distribution, and reproduction in any medium, provided the original work is properly cited.

Due to the excellent performance, giant magnetostrictive actuator is used in the active vibration isolation control system. However, its hysteresis nonlinear dynamic model is too complex for engineering practical applications, so it is necessary to establish an accurate and easy-to-use model. Based on Simulink/Simcape, a magnetic circuit model and a nonlinear dynamic physical model of the giant magnetostrictive actuator are developed. In the optimization of the magnetic circuit, the uniform distribution and the magnetic energy utilization of the giant magnetostrictive actuator are taken as the optimization objective, and the design criteria of the magnetic circuit are given. The hysteresis performance between the current and the magnetization is analyzed by simulating the magnetic circuit model. From the perspective of energy conservation, a linear magnetostrictive model which can reflect the effects of the frequency doubling and preload is established. Finally, the accuracy of the nonlinear dynamic physical model for the giant magnetostrictive actuator is verified by an experiment. The results show that the physical model agrees well with the experiment results not only under the quasistatic operating conditions but also under dynamic operating conditions. The error of the output displacement of the GMA under step response is less than  $0.6\ \mu\text{m}$ .

## 1. Introduction

With the advancement of active control on vibration, giant magnetostrictive actuator (GMA), which has the advantages of fast response, high reliability, and high precision, is applied in the high-precision active vibration isolation platform [1–6]. In order to design, evaluate, and control the performance of the GMA, it is necessary to establish its accurate mathematical model [3, 7–10].

The earliest model of the GMA is a linear piezomagnetic equation without considering the effects of stress, temperature, and hysteresis [11]. The linear piezomagnetic coefficient is used to measure the magnetic mechanical coupling characteristics of giant magnetostrictive materials. Experiments and applications show that it is feasible to use this model to describe the output performance of the GMA if a certain preload and bias magnetic field are applied to a GMM rod under low frequency and weak magnetic drive

[4]. However, because its core component GMM is the ferromagnetic material, the intrinsic hysteresis nonlinearity exists in its magnetization process, and when the driving frequency is slightly higher, it is also affected by the eddy current loss and other electromagnetic losses. Therefore, when the driving magnetic field intensity and frequency are slightly higher, the accuracy of the model is not high. So, it is necessary to analyze the performance of the GMA based on the hysteresis nonlinear dynamic model considering the influence of the eddy current.

At present, the models used to describe the hysteresis nonlinearity of a magnetostrictive actuator are mainly divided into three categories: The first category is the phenomenological model, which is a purely mathematical model without any physical mechanism, such as the Preisach hysteresis model [11]. The second category is the physical model based on physical mechanisms, such as the Jiles–Atherton model based on the magnetization

mechanism and the free energy hysteresis model based on the thermodynamic theory [12–13]. The third category is the data-driven model based on the experimental data and the artificial intelligence algorithm, such as the neural network model [7].

The Preisach hysteresis model is a mathematical model without any physical mechanism, which has a strong prediction ability for the hysteresis nonlinearity. Clark et al. applied it to describe the hysteresis of the GMA, but this model can only describe the hysteresis characteristics under a quasi-static driving magnetic field. With the increase in the driving frequency, the error of this model becomes large [11]. In order to study and control the dynamic nonlinearity of the GMA, Tan and Baras developed a dynamic Preisach hysteresis model based on the phenomenological theory of the electrocircuit and gave the dynamic compensation control method of the GMA based on the inverse model of this model [14]. The results show that compared with the static Preisach hysteresis model, this model has higher tracking control performance, and its application range can reach 200 Hz. In order to control the GMA in real time, Yang used the Prandtl–ishlinskii model, which is an upgraded version of the Preisach model, for modelling and compensation control for the hysteresis of the GMA. Through the experiment, the maximum prediction error of this model is  $0.146\ \mu\text{m}$ . The accuracy of this compensation control can reach  $0.309\ \mu\text{m}$  [15]. The Prandtl–ishlinskii model has the advantages of small computation, simple structure, and convenient inversion, so it especially meets the requirements of real-time control of the GMA.

The Jiles–Atherton model is a hysteresis model based on the Weiss molecular field theory and the domain wall motion mechanism. It has relatively few structural parameters and a clear magnetization physical mechanism. Sablik and Jiles developed this model to analyze the magnetic mechanical coupling effect caused by stress and the coupling effect of magnetization and magnetostriction. Later, Jiles added the eddy current loss and other loss terms to the Jiles–Atherton hysteresis model to describe the magnetization of ferromagnet driven by a medium or a low frequency alternating magnetic field [11, 16–22]. Wang applied this modified model to describe the performance of the GMA, established a GMA dynamic model considering the eddy current effect and the stress' change, and identified the model parameters by a hybrid genetic algorithm [5]. Calkins et al. improved the Jiles–Atherton hysteresis model from the perspective of energy so that it can describe the hysteresis characteristics of the main loop and the symmetrical small loop of the GMA under different conditions. Chakrabarti and Dapino derived the relationship between the radial magnetic field distribution of the GMM rod and the driving frequency from Maxwell equations, by substituting the average radial magnetic field intensity of the GMM rod into the Jiles–Atherton hysteresis model. The GMA dynamic hysteresis model considering the influence of the driving frequency is given. The application range of this model can reach 2 kHz [3].

Smith studied hysteresis from the perspective of thermodynamics and proposed the free energy hysteresis model. Because it is similar to the mathematical form of the Preisach model, it is also called the physical Preisach model.

Chakrabarti and Dapino applied the physical Preisach model to model the hysteresis of the GMA, which presented a good performance [3]. On the basis of this model and Tan Xiaobo's phenomenological theory of the electrocircuit, Tian et al. established a dynamic free energy hysteresis model, whose application range was 300 Hz [13]. Zheng et al. studied the coupling effects such as the preload, the temperature, and the alternating magnetic field on the dynamic characteristics of the GMA. Based on the Gibbs free energy theory, they established a new model to describe magnetic-mechanical coupling characteristics of the GMM rod driven by a strong magnetic field [16].

Because the neural network can fit any complex nonlinearity with high accuracy, it was used to accurately describe and control the dynamic nonlinear of the GMA. Cao et al. proposed a GMA control strategy based on the dynamic recurrent neural network model [7]. In addition, the RBF neural network and the Fuzzy-RBF neural network were also used to model and control the dynamic characteristics of the GMA by the online hysteresis compensation control method. Li et al. applied the small quadratic support vector machine theory to model the hysteresis of the GMA. This maximum relative error of the model was about 2.5%. Compared with the traditional neural network model, this model requires less experimental data [19]. Although the neural network hysteresis model has many advantages, it is only a nonlinear fitting of the experimental data and cannot be used to design and optimize the performance of the GMA.

To sum up, the first and the third types of models cannot reflect the physical mechanism of the GMA and the influence of the physical parameters on the performance of the GMA cannot be studied through the model. The second type of model is the implicit equation groups in differential form. The formulas are complex and need to be solved by programming, which is difficult for engineering practical applications. Therefore, an accurate and simple modeling method is very necessary for the engineering application of the GMA [20–26]. With the development of computer software, the physical modeling method based on simulation software is more and more welcomed by the engineers and technicians. The physical modeling method only needs to connect and assemble the basic physical components to the module block diagram according to the schematic diagram, so as to establish a complex multidisciplinary system model and carry out simulation calculation and in-depth analysis on this basis, so as to avoid cumbersome mathematical modeling. In this work, the dynamic hysteresis nonlinear physical model of the GMA is given based on the Simulink Physical Modeling Toolbox (Simcape), and its performance is analyzed. In addition, the magnetic circuit physical model of the GMA is also developed based on Simcape, which includes all magnetic resistances in the magnetic circuit.

The contents are organized as follows: Section 2 introduces the configuration and the working principle of the GMA, while Section 3 presents a physical model and optimization of the magnetic circuit. Section 4 shows the magnetomechanical model. Section 5 shows the kinetic models of the GMA. Section 6 discusses simulation and the experiment.

## 2. Configuration and Working Principle of the GMA

The configuration of the GMA is shown in Figure 1. It mainly consists of an annular permanent magnet, a giant magnetostrictive material (GMM) rod, a coil, a spring, and an output rod. The annular permanent magnet is used to provide a longitudinal bias magnetic field to improve the sensitivity of the GMM rod and eliminate frequency doubling. In order to save cost, the annular permanent magnets are stacked with standard magnet rings, as shown in Figure 2. The coil is used to generate the control magnetic field to drive the GMA output displacement. The spring is used to apply a prestress on GMM because a larger magnetostrictive strain can be obtained with a same magnetic field when GMM is compressed.

Figure 3 illustrates the prototype of the GMA. The conversion from the current to the displacement of the GMA involves three energy conversion processes, namely, the conversion from electric energy to magnetization energy, the conversion from magnetization energy to strain energy, and the conversion from strain energy to mechanical energy. Therefore, the GMA's model includes the magnetization submodel describing the conversion from electric energy to magnetization energy, the magnetostriction submodel from magnetization energy to strain energy, and the mechanical submodel from strain energy to mechanical energy. In addition, when the driving frequency is high, the effect of the eddy current on magnetization should be included in the magnetization model.

## 3. Physical Model and Optimization of the Magnetic Circuit

**3.1. Optimization of the Magnetic Circuit.** GMM is the core component of the GMA, which is driven by a magnetic field. Both the magnetic field uniformity and the magnetic energy utilization on the GMM rod seriously affect the performance of the GMA [27]. Under the same ampere-turns, the more uniform the magnetic field is, the stronger the magnetic field intensity is, the better the performance of GMM is, and the higher the efficiency is.

Assuming the magnetic flux density of the annular permanent magnet is 0.2 T, the length of the GMM rod is 80 mm, the diameter is 10 mm, the number of coil turns is 1200, the control current is 1 A, the coil's length is 70 mm, 80 mm, and 90 mm, respectively, and the inner diameter of the coil is 12 mm. The linear "Hard" magnetic material is used for permanent magnets. The nonlinear "Soft" magnetic material model is used for GMM. The linear "Soft" magnetic material is used for other magnetic resistances in the magnetic circuit.

Based on the three-dimensional structure of the GMA, through the magnetic field finite element analysis with ANSYS/Maxwell, the three-dimensional electromagnetic field distribution in the GMA can be obtained, as shown in Figure 4.

Figure 4 shows that under the same number of ampere-turns, the internal magnetic field strength of the GMM rod changes with the coil's length. In order to clearly study the

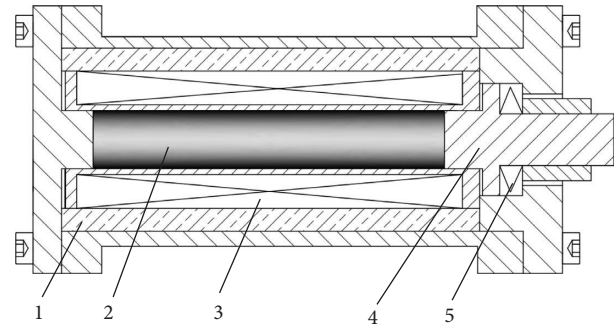


FIGURE 1: The configuration diagram of the GMA. (1) permanent magnet; (2) GMM rod; (3) coil; (4) output rod; and (5) Spring.



FIGURE 2: The photograph of annular permanent magnet.



FIGURE 3: The prototype of the GMA.

magnetic field distribution in the GMM rod, only the magnetic field on the GMM rod is displayed. Figure 5 is the magnetic field distribution of the GMM rod in Figure 4(a). Figure 5 shows that the magnetic field distributions in the GMM rod are uneven. The magnetic field strength is extracted on the GMM axis in Figure 4, and the distribution of the magnetic field strength on the axis of the GMM rod under different lengths of the coil can be obtained as shown in Figure 6. It can be seen from Figure 6 that when the coil's length is 70 mm or 80 mm, the magnetic field strength on the axis of the GMM rod is strong in the middle and weak at both ends. When the coil's length is 90 mm, the magnetic field strength on the GMM axis is weak in the middle and strong at both ends.

The magnetic field intensity on the end face ( $Z=0$ ) and the middle section ( $Z=40$ ) of the GMM rod are extracted from Figure 4. The distribution law of the radial magnetic field intensity in the GMM rod is shown in Figures 7 and 8. They show that the radial distribution of the magnetic field in the GMM is also uneven.

The discretization form for the degree of the magnetic field unevenness formula is defined as follows:

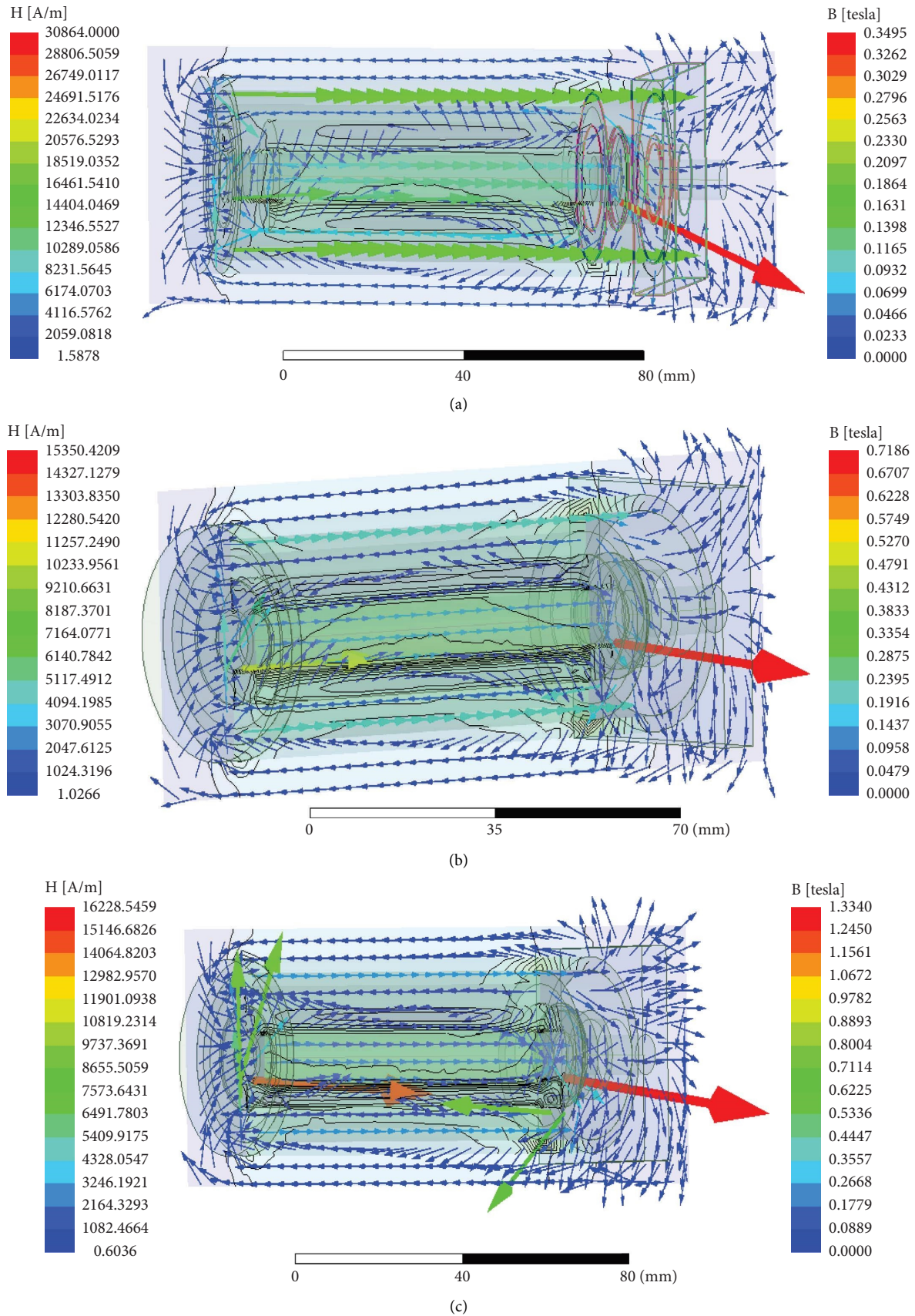


FIGURE 4: 3D magnetic field distribution in the GMA under different GMM rod lengths. (a) Magnetic field distribution in the GMA when the length of the GMM rod is 70 mm. (b) Magnetic field distribution in the GMA when the length of the GMM rod is 80 mm. (c) Magnetic field distribution in the GMA when the length of the GMM rod is 90 mm.

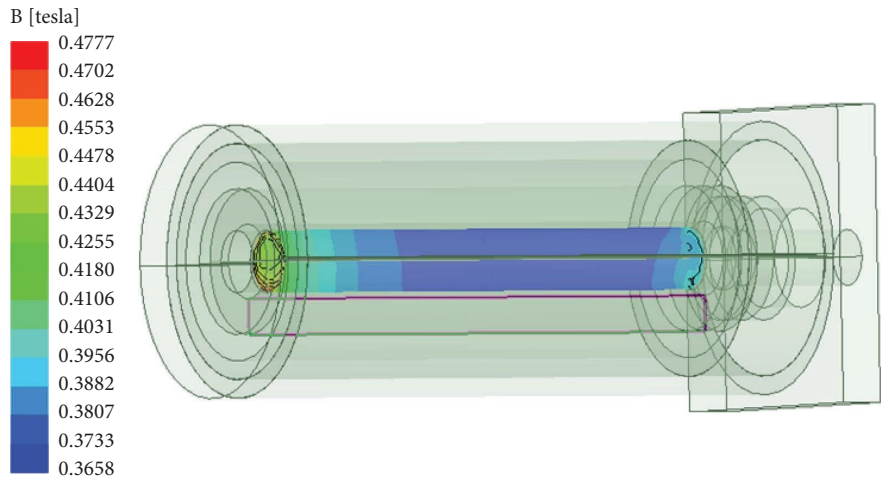


FIGURE 5: 3D magnetic field distribution in GMM.

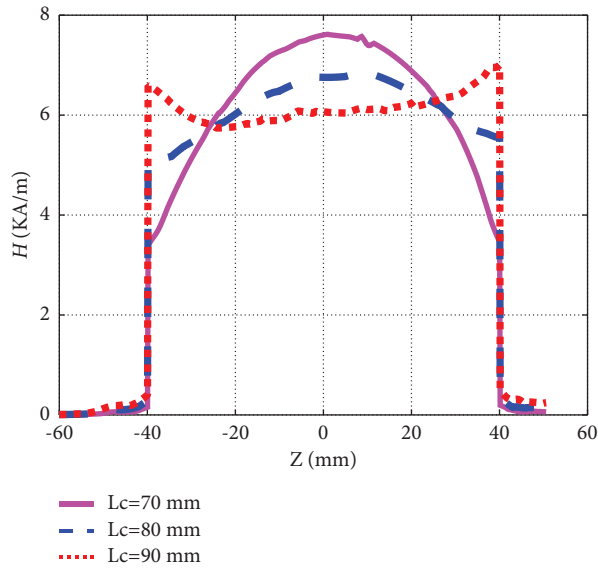


FIGURE 6: Magnetic field on the axis of GMM rod with the coil's diameter of 10 mm.

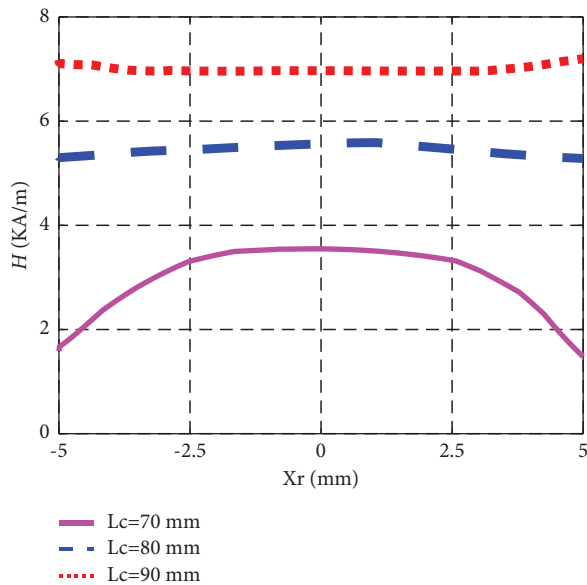


FIGURE 7: Radial magnetic field of GMM rod with the coil's diameter of 10 mm ( $Z = 40$ ).

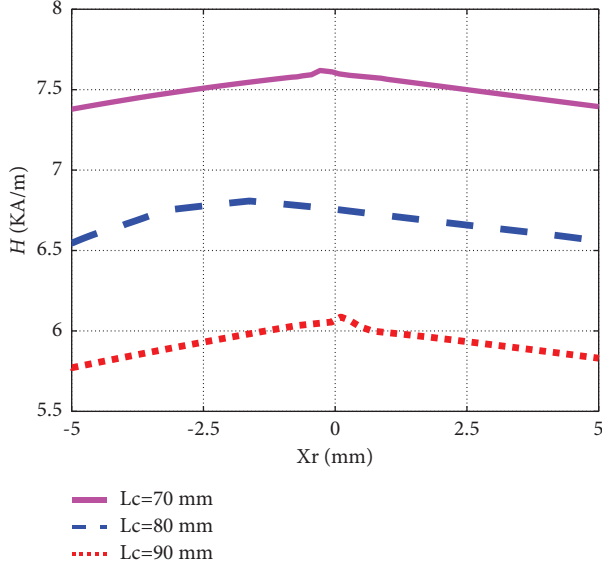


FIGURE 8: Radial magnetic field of GMM rod with the coil's diameter of 10 mm ( $Z = 0$ ).

$$\delta_B = \frac{\max(H_i) - \min(H_i)}{\bar{H}}, \quad (1)$$

where  $\bar{H}$  is the average magnetic field intensity, and it can be obtained as follows:

$$\bar{H} = \frac{\sum_{i=1}^n H_i}{n}, \quad (2)$$

where  $dU = dQ + dW$  is the number of the observation points.

Substituting the numerical simulation results of the magnetic field intensity in Figures 6 to 8 into equations (1) and (2), the calculated results of the axial average magnetic field intensity and the degree of the magnetic field unevenness under different lengths of the coil are shown in Tables 1 and 2.

It can be seen from Tables 1 and 2 that under the same number of ampere-turns, with the increase in coil length, the average magnetic field intensity on the center line decreases, but the average magnetic field intensity in the GMM rod increases and the degree of the magnetic field unevenness decreases. Therefore, from the two aspects of magnetic energy utilization and magnetic field uniformity, under the same ampere-turns, the longer the coil's length is, the better the performance is. So, the length of the coil should be longer than the length of the GMM rod. However, the improvement of GMA's performance is very small, as the coil's length is changing from 80 mm to 90 mm.

Assuming that the coil's length is 80 mm, the coil's radius is 6 mm, 7 mm, and 8 mm, respectively. According to the numerical simulation of the magnetic field, the magnetic field intensity on the center line, the end face, and the middle section of the GMM rod under the same ampere-turns are shown in Figures 9–11. It can be seen that when the coil's inner diameter is Figure 10 different, the magnetic field distribution is also different. The magnetic field intensity on the center line is high in the middle and low at both ends,

TABLE 1: Average magnetic field intensity under different coil lengths.

Coil lengths (mm)	70	80	90
$\bar{H}$ in the center line	6.2863	6.1610	6.1443
$\bar{H}$ in the end face	3.0365	5.4516	6.9958
$\bar{H}$ in the midsection	7.5021	6.6965	5.9312
$\bar{H}$ in GMM	5.6083	6.1030	6.3571

TABLE 2: Nonuniformity of magnetic field distribution under different coil lengths.

Coil lengths (mm)	70	80	90
$\delta_B$ in the center line	0.6701	0.2861	0.2049
$\delta_B$ in the end face	0.6818	0.0557	0.0345
$\delta_B$ in the midsection	0.0320	0.0390	0.0531
$\delta_B$ in GMM	1.0949	0.2889	0.2293

and the magnetic field intensity on the middle section is high in the middle and low at both ends, but it is high in the middle and low at both ends at the coil's inner diameter of 6 mm. Figure 11 shows that the smaller the inner diameter of the coil is, the stronger the magnetic field intensity in the middle section is.

By substituting the data of Figures 9–11 into equations (1) and (2), it can be seen that the average magnetic field intensity and the unevenness of GMA with the coils having different inner diameters under the same ampere-turns are shown in Tables 3 and 4. It can be seen from Table 3 that with the increase in coil's inner diameter, the average magnetic field intensity on the GMM decreases, but the magnetic field distribution is more uniform. When the inner diameter of the coil is large, the coil's resistance and inductance will increase under the same number of turns, resulting in more heat and affecting the dynamic performance of the GMA. Therefore, considering the magnetic energy utilization and structural constraints, the inner diameter of the coil is chosen as 6 mm.

From the above analysis, it can be seen that when the number of ampere-turns is constant, the longer the coil's length is, the greater the average magnetic field intensity is, while the smaller the nonuniformity is. The smaller the coil's inner diameter is, the greater the magnetic field intensity is, while the more uneven the magnetic field distribution is. Therefore, from the aspects of the magnetic energy utilization and the magnetic field uniformity, the design of the magnetic circuit in the GMA needs to meet the following requirements: (1) The magnetic circuit is preferably closed; (2) The length of the coil (excluding the coil frame) is greater than the length of the GMM rod, and the inner diameter is close to the diameter of the GMM rod; (3) The permeability of other materials on the magnetic circuit should be much greater than the GMM rod.

3.2. *Magnetization Physical Model Based on the Magnetic Circuit.* Figure 12 shows the magnetic circuit of the GMA, which can be obtained from Figure 1. Based on Figure 12, the magnetic circuit physical model of the GMA in Simulink/

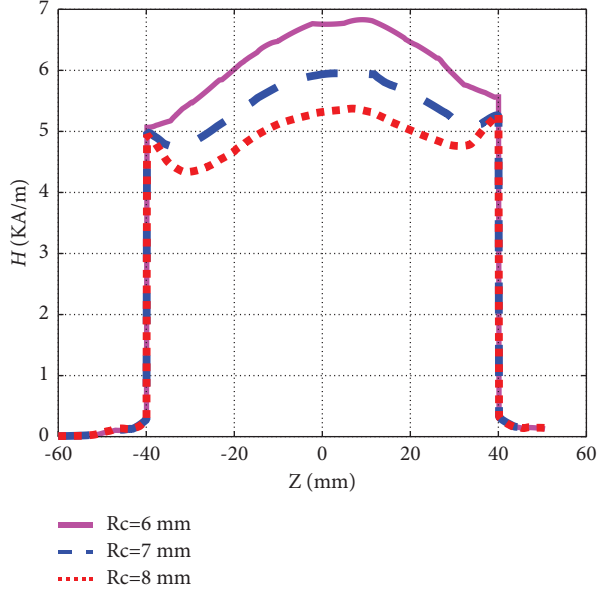


FIGURE 9: Magnetic field on the axis of GMM rod with the coil's length of 80 mm.

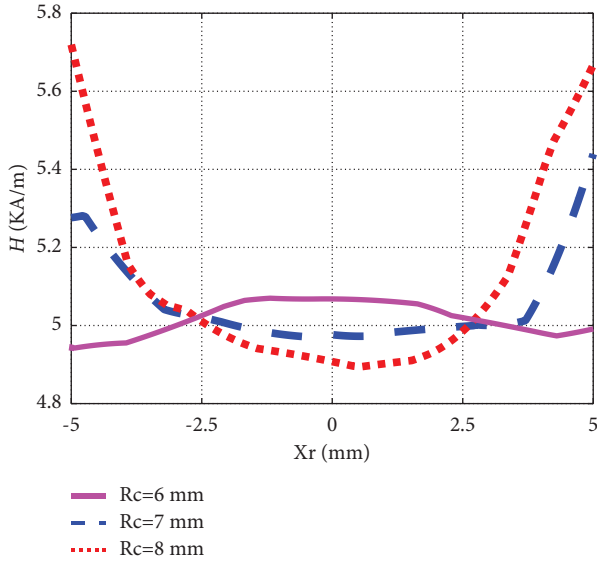


FIGURE 10: Radial magnetic field of GMM rod with the coil's length of 80 mm ( $Z = 40$ ).

Simcape can be given as shown in Figure 13. The physical meanings of magnetic elements in Figure 13 are described in Table 5.

3.3. *Simulation.* The simulation parameters in Table 6 are substituted into the GMM magnetization simulation model shown in Figure 13. Assuming that the amplitude of the control current is 1 A, the driving frequency is 1 Hz and the magnetic flux of the bias magnetic field is 0 and 0.5 T, respectively. The relationship curves between the magnetization and the control current are shown in Figure 14 under different bias magnetic fields. Figure 14 shows that

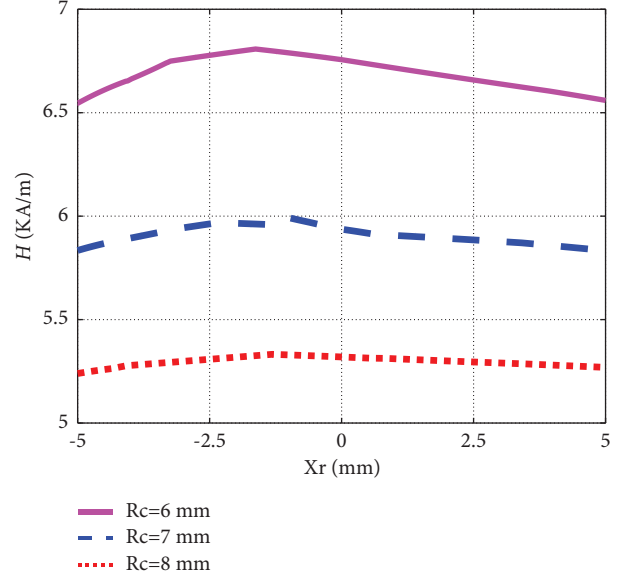


FIGURE 11: Radial magnetic field of GMM rod with the coil's length of 80 mm ( $Z = 0$ ).

TABLE 3: Average magnetic field intensity under different coil inner diameters.

Coil radius (mm)	6	7	8
$\bar{H}$ in the center line	6.1610	5.5670	5.1052
$\bar{H}$ in the end face	5.4516	4.8110	4.7540
$\bar{H}$ in the midsection	6.6965	5.9886	5.4717
$\bar{H}$ in GMM	6.1030	5.5605	5.2090

TABLE 4: Nonuniformity of magnetic field distribution under different coil diameters.

Coil radius (mm)	6	7	8
$\delta_B$ in the center line	0.2861	0.2217	0.1593
$\delta_B$ in the end face	0.0557	0.0603	0.1282
$\delta_B$ in the midsection	0.0390	0.0241	0.0190
$\delta_B$ in GMM	0.2889	0.2160	0.1328

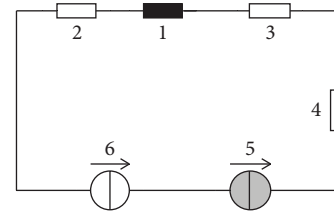


FIGURE 12: The magnetic circuit of the GMA. (1) GMM's magnetic reluctance; (2) rear end cover's magnetic reluctance; (3) front end cover's magnetic reluctance; (4) outer housing's magnetic reluctance; (5) magnetic flux of permanent magnet; (6) magnetic flux of the coil.

increasing the bias magnetic field can greatly reduce the hysteresis nonlinearity, but the magnetic susceptibility is decreased. The control current changes from  $-1$  A to  $1$  A, and the magnetization changes by  $152068$  A/m under the

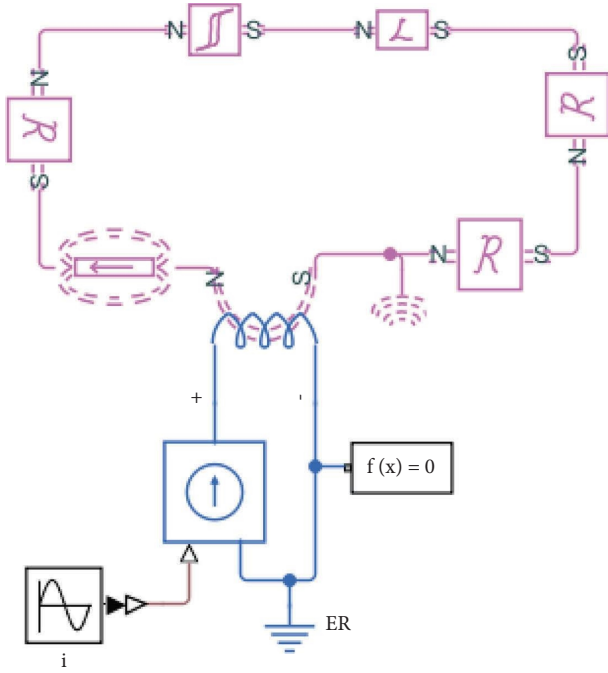


FIGURE 13: The physical model of the magnetic circuit.

TABLE 5: Description of magnetic components in the physical model.





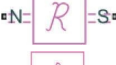
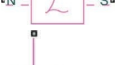

Magnetic components	Meanings
	Flux of permanent magnet
	GMM's magnetic reluctance with magnetic hysteresis
	Controlled current Source, which is driven by input signal
	Coil, which is an electromagnetic energy conversion device
	Other magnetic reluctances in the magnetic circuit
	Eddy currents in GMM are caused by time varying magnetic fields
	Magnetic reference

TABLE 6: Simulation parameters of the magnetization model for GMM.

Parameter	Value
GMM rod length	80 mm
Reversibility coefficient	0.1
Shell permeability	1000
Initial permeability	10
GMM rod diameter	10 mm
Turn ratio	2000
Bias flux	0.0048 Wb
Pincoupling coefficient	6000 A/m

bias magnetic field of 0, while the magnetization changes by 69450 A/m under the bias magnetic field of 0.01 Wb. In addition, it can be seen from Figure 14(b) that the magnetization curve is no longer symmetrical about the center after the bias magnetic field is applied.

#### 4. Magnetostrictive Model of GMM

The microphysical mechanism of the magnetostriction effect is very complex, but it can be explained macroscopically from the perspective of thermodynamics.

The GMM rod satisfies the first law of thermodynamics during magnetization.

$$dU = dQ + dW, \quad (3)$$

where  $dU$  is the increment of internal energy of the GMM rod;  $dQ$  is the increment of heat absorbed by the GMM rod during magnetization; and  $dW$  is the increment of work performed by the outside world on the GMM rod.

According to the second law of thermodynamics,

$$dQ = TdS, \quad (4)$$

where  $T$  is the thermodynamic temperature of the GMM rod and  $dS$  is the change of entropy of the GMM rod.

The increment of work done by the outside world to the GMM rod consists of the magnetization work done by the external magnetic field to the GMM rod and the volume work done by the GMM rod due to volume change. The magnetization work is also positive, and the volume work is also negative. Therefore,

$$dW = \mu_0 H_e dM - \sigma d\lambda, \quad (5)$$

where  $H_e$  is the effective magnetic field applied inside the GMM rod and  $M$  is the magnetization.  $\sigma$  and  $\lambda$  are the stress and the strain caused by the magnetostrictive effect, respectively.

The effective magnetic field in the GMM rod is not equal to the external magnetic field applied to the GMM rod. The function of the external magnetic field is only to change the direction of the magnetic moment formed by spontaneous magnetization and make the magnetic moment rotate in a direction parallel to the external magnetic field. Sablik and Jiles believe that under the action of axial stress, the effective magnetic field inside the GMM rod is given as follows:

$$H_e = H + \alpha M + \frac{9\lambda_s \sigma_0}{2\mu_0 M_s^2} M = H + \tilde{\alpha} M, \quad (6)$$

where  $dU = TdS + \mu_0 H_e dM + \sigma d\lambda$  is the preloading stress applied on the GMM rod;  $dU = TdS + \mu_0 H_e dM + \sigma d\lambda$  is the molecular field parameter of magnetic moment interaction;  $dU = TdS + \mu_0 H_e dM + \sigma d\lambda$  and  $dU = TdS + \mu_0 H_e dM + \sigma d\lambda$  are the saturation magnetostriction and saturation magnetization of the GMM rod;  $dU = TdS + \mu_0 H_e dM + \sigma d\lambda$  is vacuum permeability.

Simultaneous equations (3)~(5) can be obtained.

$$dU = TdS + \mu_0 H_e dM - \sigma d\lambda. \quad (7)$$



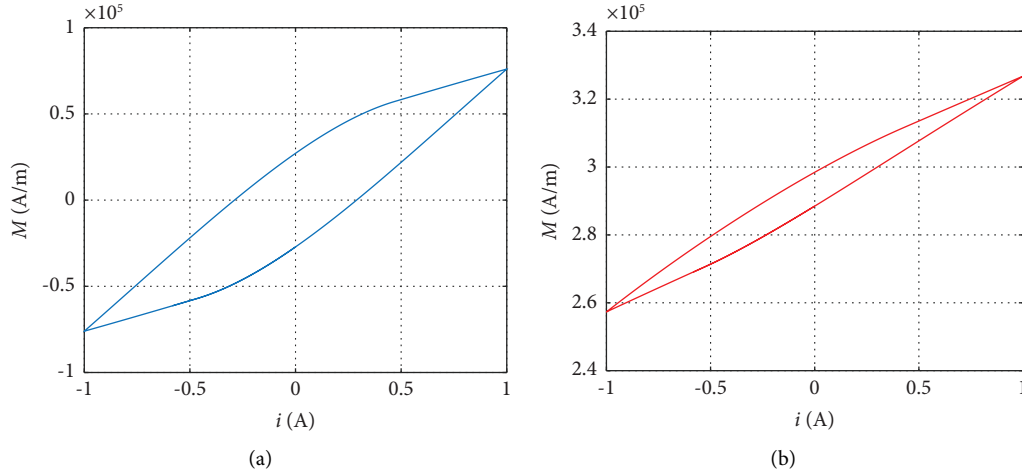


FIGURE 14: Relationship curves between the control current  $i$  and magnetization  $M$ . (a) The  $i$ - $M$  curve when  $B_0 = 0$ . (b) The  $i$ - $M$  curve when  $B_0 = 0.5$  T.

Gibbs free energy is written as follows:

$$G(T, \sigma, M) = U - TS + \sigma\lambda. \quad (8)$$

Hence, total differential form of Gibbs free energy is written as follows:

$$dG = dU - TdS - SdT + \sigma d\lambda + \lambda d\sigma. \quad (9)$$

Substituting equation (7) into equation (9) yields

$$dG = -SdT + \lambda d\sigma + \mu_0 H_e dM. \quad (10)$$

And the total differential of Gibbs free energy can be written as follows:

$$dG = \frac{\partial G}{\partial T} dT + \frac{\partial G}{\partial \sigma} d\sigma + \frac{\partial G}{\partial M} dM. \quad (11)$$

Comparing equation (10) with equation (11) yields

$$\begin{cases} \frac{\partial G}{\partial \sigma} = \lambda, \\ \frac{\partial G}{\partial M} = \mu_0 H_e. \end{cases} \quad (12)$$

Since the second-order mixed partial derivatives are independent of the derivation order under continuous conditions,

$$\frac{\partial}{\partial M} \left( \frac{\partial G}{\partial \sigma} \right) = \frac{\partial}{\partial \sigma} \left( \frac{\partial G}{\partial M} \right). \quad (13)$$

Substituting equation (12) into equation (13) yields

$$\frac{\partial \lambda}{\partial M} = \mu_0 \frac{\partial H_e}{\partial \sigma}. \quad (14)$$

Thus,

$$\partial \lambda \cdot \partial \sigma = \mu_0 \partial M \cdot \partial H_e. \quad (15)$$

Equation (15) shows that the change of the magnetization state in the GMM rod will cause the change of the strain state. The minus sign in the formula indicates that with the increase in magnetization, the GMM rod works externally and it is in an extended state.

The relationship between stress and strain is given by the following equation:

$$\partial \sigma = E^H \cdot \partial \lambda, \quad (16)$$

where  $E^H$  is Young's modulus of the GMM rod.

Substituting equation (16) into equation (15) and taking the square root yield

$$\partial \lambda = \sqrt{\frac{\mu_0 \partial M \cdot \partial (H + \tilde{\alpha} M)}{E^H}} = \sqrt{\frac{\mu_0}{E^H} \left( \frac{\partial H}{\partial M} + \tilde{\alpha} \right) |\partial M|}. \quad (17)$$

Integrating equation (17) yields

$$\lambda(M) = \sqrt{\frac{\mu_0}{E^H} \left( \frac{\partial H}{\partial M} + \tilde{\alpha} \right) |M|} + \varepsilon_0, \quad (18)$$

where  $\varepsilon_0$  is the strain caused by a preload stress and a thermal deformation.

It can be obtained from Section 3.3 that the magnetic susceptibility of GMM is not a constant, so  $(\partial H / \partial M)$  is not a constant. Therefore, the relationship between the magnetostriction and the magnetization shown as equation (18) is not linear.

It can be seen from equation (18) that the magnetostriction is always positive no matter whether the magnetization is positive or negative. In engineering applications, in order to obtain a GMA with bidirectional output, the bias magnetic field is always applied in the GMM rod. In addition, applying a suitable bias magnetic field can improve the magnetostriction sensitivity of the GMM rod so that

a large displacement can be controlled by a small magnetic field.

After the bias magnetic field is applied and the displacement generated by the bias magnetic field is taken as the

$$\lambda(M) = \sqrt{\frac{\mu_0}{E^H} \left( \frac{\partial H}{\partial M} \Big|_{M=M_b} + \tilde{\alpha} \right)} |M| - \lambda_b = \sqrt{\frac{\mu_0}{E^H} \left[ \frac{1}{\chi(M) \Big|_{M=M_b}} + \tilde{\alpha} \right]} |M| - \lambda_b, \quad (19)$$

where  $M_b$  is the magnetization generated by the bias magnetic field and  $\lambda_b$  is the magnetostriction generated by the bias magnetic field.  $\chi(M)$  is the susceptibility of the GMM, which varies with the level of the driving magnetic field.

When the driving magnetic field is small compared with the bias magnetic field, equation (19) is reasonable. When the driving magnetic field is large, the magnetic susceptibility changes greatly, and GMM will show a serious nonlinearity, so susceptibility of the GMM rod in equation (19) needs to be given as a variable in this condition.

The relationship between magnetic field strength and magnetization is given by the following equation:

$$B = \mu_0(H + M). \quad (20)$$

Hence, equation (19) can be written as follows:

$$\lambda(M) = \sqrt{\frac{\mu_0}{E^H} \left[ \frac{1}{\chi(M) \Big|_{M=M_b}} + \tilde{\alpha} \right]} \left| \frac{B}{\mu_0} - H \right| - \lambda_b. \quad (21)$$

## 5. Kinetic Models of the GMA

A large number of experiments and theoretical studies show that when the GMA system adopts the lumped parameter model, its equivalent physical model is the mass-spring-damping system. So the kinetic model of the GMA can be equivalent to the system as shown in Figure 15, where  $m$  is the equivalent mass,  $C$  is the equivalent damping, and  $K$  is the equivalent stiffness.

Force generated by the magnetostriction is given by the following equation:

$$F_\lambda = A_G E^H \lambda(M). \quad (22)$$

The physical model from magnetization to output force can be obtained by combining equations (21) and (22), as shown in Figure 16.

Based on the working principle of the GMA, the physical submodel of the magnetic circuit, the magnetostrictive output force submodel, the equivalent mechanical submodel of the GMA, and the physical model from the control current to the output displacement of the GMA can be established, as shown in Figure 17.

reference zero point, the magnetostriction model described by equation (18) can be rewritten as follows:

## 6. Simulation and Experiment

**6.1. Simulation.** Substituting simulation parameters shown in Table 7 (the susceptibility of the GMM with the bias magnetic field of 0.2 T is 4) into the physical model in Figure 17 and assuming that the magnetic flux density of permanent magnet is 0, 0.5 T, and 0.2 T, respectively, the control current is a sinusoidal signal with the amplitude of 1 A and the frequency of 1 Hz, and the curves of GMA output displacement and the control current with time can be obtained, as shown in Figure 18.

Figure 18(a) shows that when the bias magnetic field is 0, the frequency of GMA output displacement is twice the frequency of the control current. The reason is that when the bias magnetic field is 0, GMA outputs a positive displacement under a positive or a negative control current, as shown in Figure 18(b). In order to realize the bidirectional control of the GMA, the method of applying the bias magnetic field is usually used to eliminate this “frequency doubling” phenomenon shown in Figure 18(a).

Figures 18(c) and 18(e) show that the “frequency doubling” phenomenon is gradually eliminated with the increase in the bias magnetic field. The bias magnetic field can make the GMA obtain a large displacement under the same control current. Compared with Figures 18(b), 18(d), and 18(f), it can be seen that the GMA can get a larger displacement under the same control current when the bias magnetic field is 0.2 T. So, a proper bias magnetic field can not only make the GMA bidirectional output displacement but also increase the sensitivity of the GMA.

**6.2. Experiment.** The experiment platform of GMA's output displacement is shown in Figure 19. The experimental device consists of the GMA, an eddy current displacement sensor and its regulator, a constant current power amplifier, a signal generator, and an oscilloscope. The signal generator generates a signal with adjustable amplitude and frequency to control the output current of the constant current power amplifier to drive the GMA. Its output displacement is measured by the eddy current sensor and finally displayed on the oscilloscope.

The control current is set as a sinusoidal signal with a frequency of 1 Hz and the amplitude of 0.25 A, 0.5 A, 0.8 A, and 1 A, respectively. The comparison results of the experiment and model simulation for the GMA under different driving levels are shown in Figure 20.



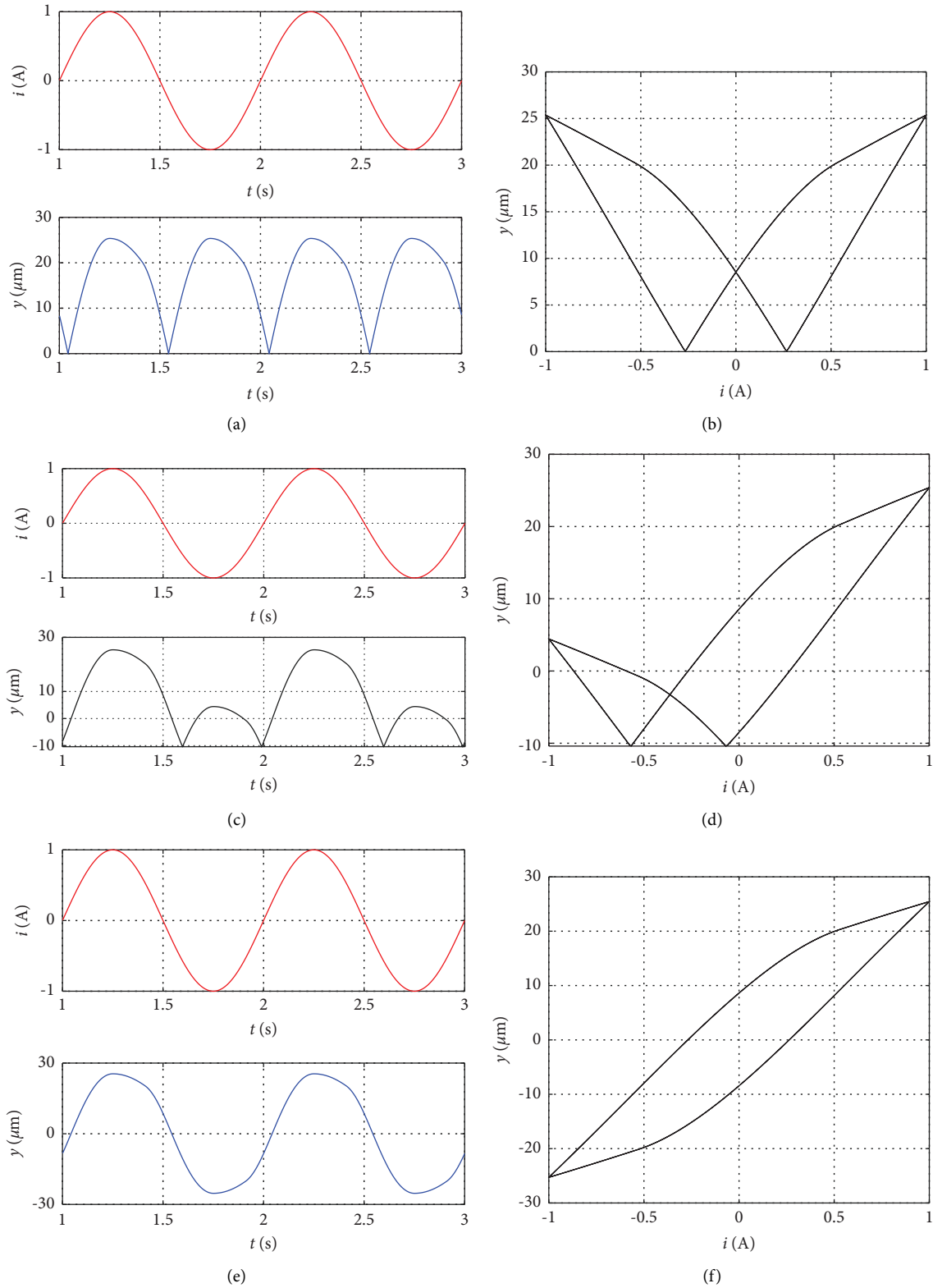


FIGURE 18: GMA output displacement under different bias magnetic fields. (a) Displacement versus time curve  $B_0 = 0$ . (b) Displacement versus current curve  $B_0 = 0$ . (c) Displacement versus time curve  $B_0 = 0.1$  T. (d) Displacement versus current curve  $B_0 = 0.1$  T. (e) Displacement versus time curve  $B_0 = 0.2$  T. (f) Displacement versus current curve  $B_0 = 0.2$  T.

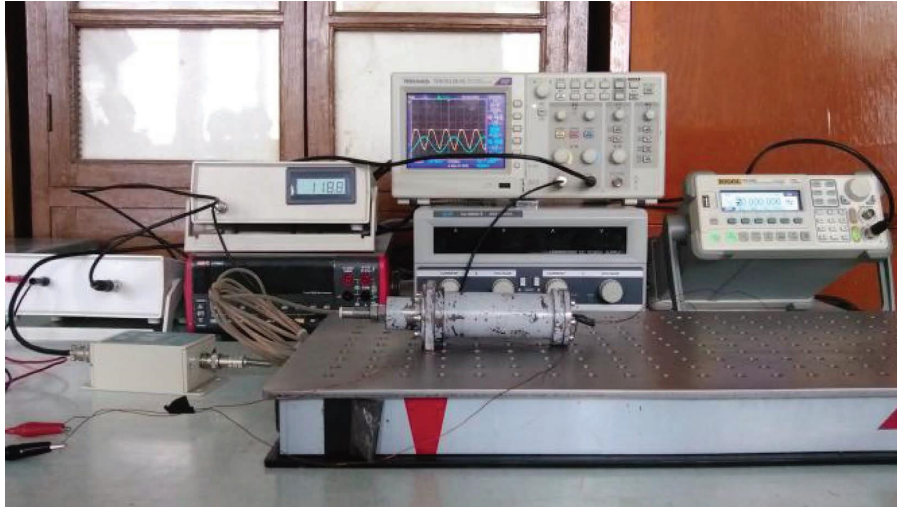


FIGURE 19: The experiment platform of GMA's output displacement.

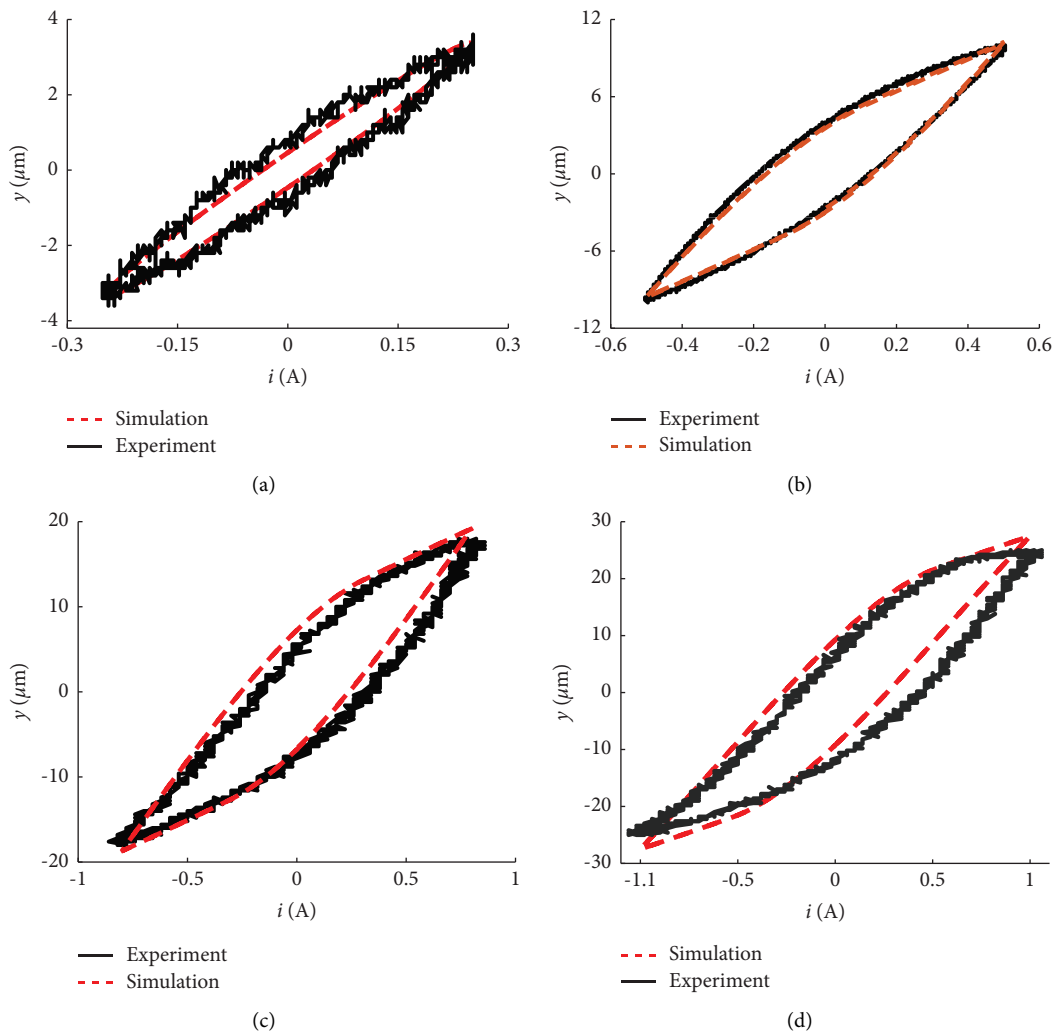


FIGURE 20: The quasistatic output displacement curve of the GMA. (a) The  $i$ - $y$  curve when  $I_m = 0.25$  A. (b) The  $i$ - $y$  curve when  $I_m = 0.5$  A. (c) The  $i$ - $y$  curve when  $I_m = 0.8$  A. (d) The  $i$ - $y$  curve when  $I_m = 1.0$  A.

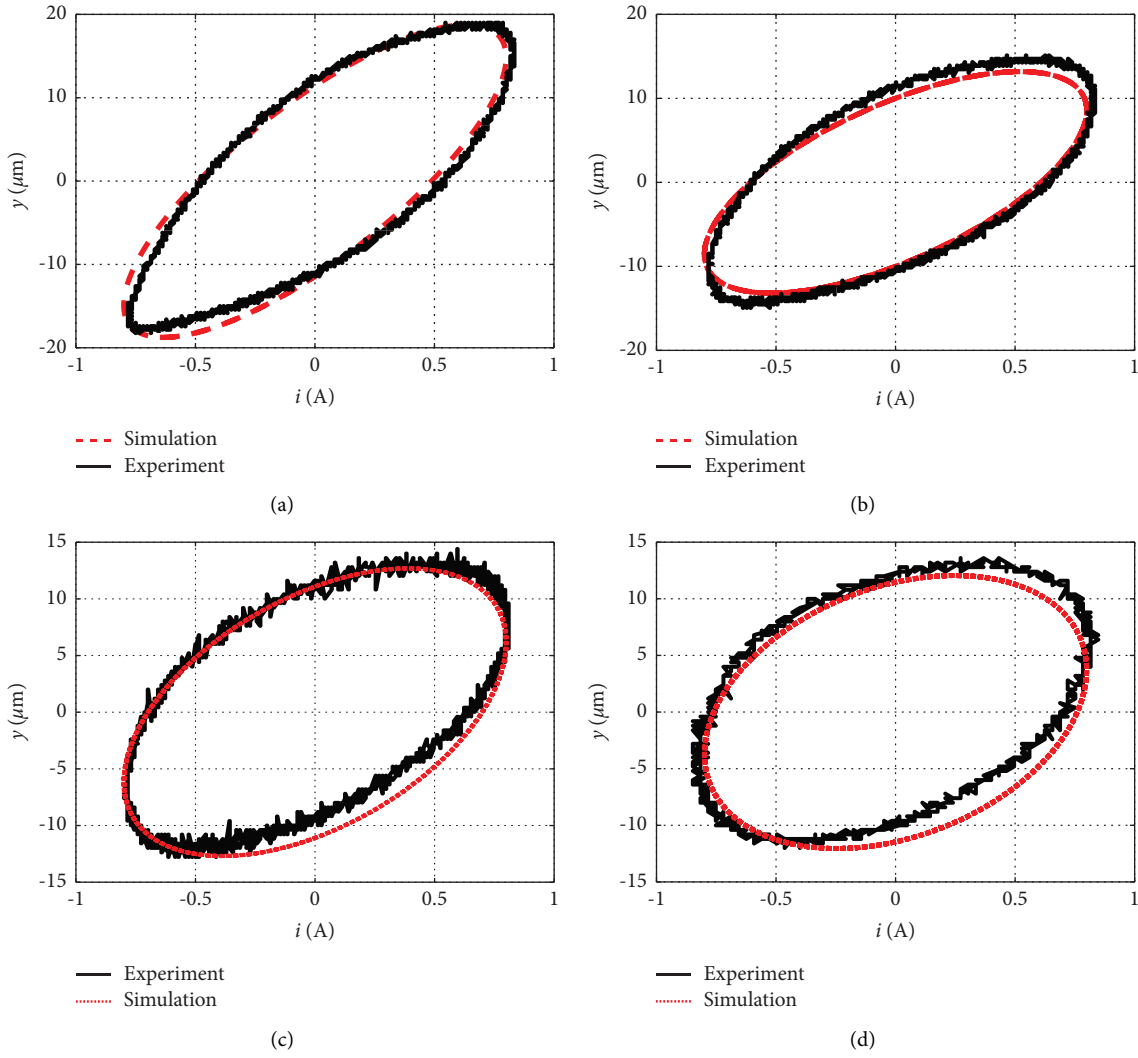


FIGURE 21: The dynamic output displacement curve of the GMA. (a) The  $i$ - $y$  curve when  $f = 50$  Hz. (b) The  $i$ - $y$  curve when  $f = 100$  Hz. (c) The  $i$ - $y$  curve when  $f = 150$  Hz. (d) The  $i$ - $y$  curve when  $f = 200$  Hz.

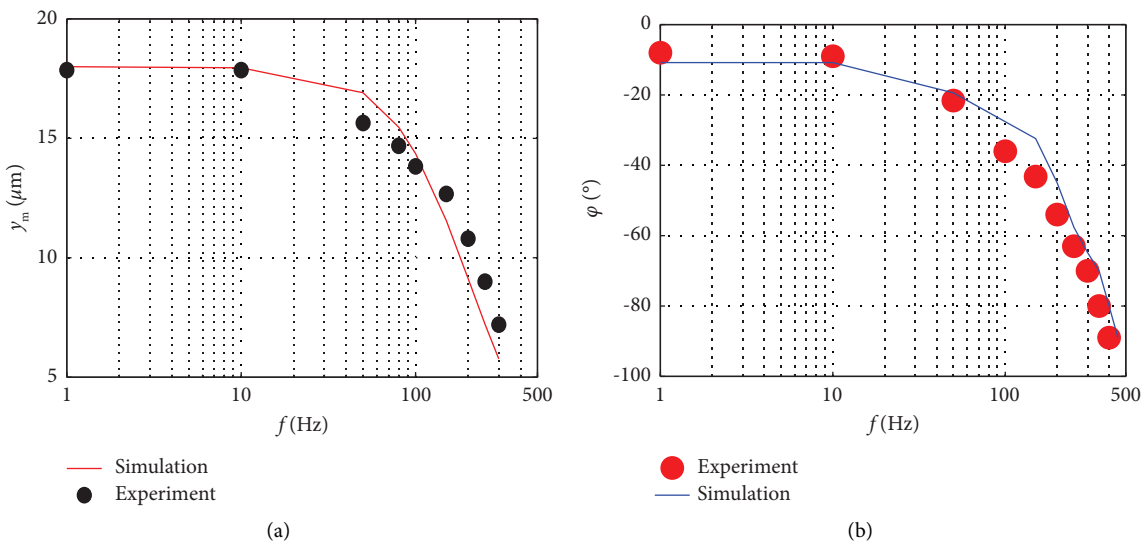


FIGURE 22: Frequency response of the GMA. (a) The amplitude-frequency curve. (b) The phase-frequency curve.

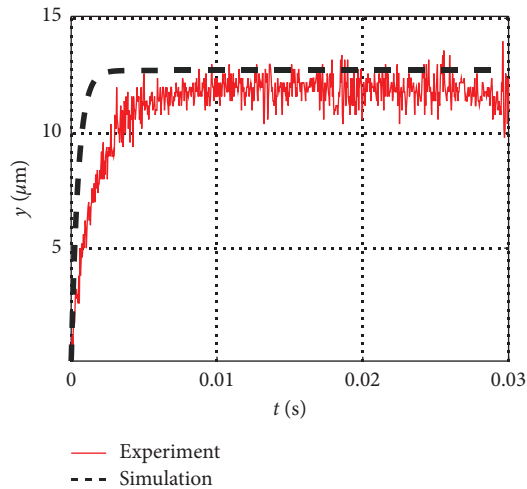


FIGURE 23: Step response of the GMA.

GMA decreases with the increase in frequency, while the phase lag relative to the input control current increases.

Setting the amplitude of the control current as 0.8 A and changing the frequency, the amplitude-frequency curve and the phase-frequency curve of the GMA can be obtained by simulation and experiments, as shown in Figure 22. The result shows that the amplitude bandwidth of the GMA is about 150 Hz and the phase bandwidth can reach to 400 Hz.

The experimental curve of the step response for the GMA can be obtained by setting the square wave signal with the control current amplitude of 0.5 A and the frequency of 1 Hz. The comparison with the simulation curve is shown in Figure 23.

It can be seen from Figure 23 that the rise time of the measured curve for the GMA is less than 5 ms and the average value of the steady-state value is about 12  $\mu\text{m}$ . The rise time of simulation is less than 2 ms, and the steady-state value is 12.6  $\mu\text{m}$ . So, the error is 0.6  $\mu\text{m}$ . The error of response time is large, which causes by slow response of the constant current power amplifier.

## 7. Conclusions

In order to make the GMA convenient to use in the practical engineering application, a nonlinear dynamic physical model of the GMA is developed. By simulation and the experiment, some conclusions are as follows:

- (1) In order to improve the magnetic field uniformity and the magnetic energy utilization on the GMM rod, the magnetic circuit of the GMA must be closed, the length of the coil should be greater than the length of the GMM rod, and the inner diameter of the coil should be close to the diameter of the GMM rod.
- (2) Under a proper bias magnetic field, the frequency doubling of the GMA can not only be eliminated but also a larger magnetostrictive strain can be obtained with the same magnetic field.
- (3) When the magnetic susceptibility is large, the magnetostrictive strain is small under the same magnetic field.

Under the zero bias magnetic field, the output displacement of the GMA is insensitive at the initial section.

- (4) The model is in good agreement with the experiment, when the GMA is driven by the low and medium magnetic fields. The error of the output displacement of the GMA under step response is less than 0.6  $\mu\text{m}$ .
- (5) The effect of the eddy current is considered in the physical model. So, it can accurately describe the complex hysteresis behavior of the GMA not only under the quasistatic operating conditions but also under dynamic operating conditions of less than 200 Hz.

## Data Availability

The data are attached in the figures and tables in the article.

## Conflicts of Interest

The author declares that there are no conflicts of interest.

## Acknowledgments

This work was supported by the Natural Science Foundation of Henan Province (grant no. 232300420085).

## References

- [1] Y. C. Zhu, Z. Y. Wang, and S. Fei, "Development of a magnetostrictive material-based electro-hydrostatic actuator with an active rotary rectifying valve," *Proceedings of the Institution of Mechanical Engineers - Part I: Journal of Systems & Control Engineering*, vol. 233, no. 8, pp. 994–1008, 2019.
- [2] M. L. Tao, D. F. Chen, and Q. G. Lu, "Eddy current losses of giant magnetostrictors," *Modeling and Experimental Analysis*, vol. 48, no. 13, pp. 146–151, 2012.
- [3] S. Chakrabarti and M. J. Dapino, "A dynamic model for a displacement amplified magnetostrictive driver for active mounts," *Smart Materials and Structures*, vol. 19, no. 5, Article ID 055009, 2010.
- [4] Y. Zhu, Y. Li, and Y. S. Li, "A hysteresis nonlinear model of giant magnetostrictive transducer," *Journal of Intelligent Material Systems and Structures*, vol. 26, no. 16, pp. 2242–2255, 2015.
- [5] B. Zhang, K. Jin, Y. Kou, X. Zheng, and Y. Kou, "The model of active vibration control based on giant magnetostrictive materials," *Smart Materials and Structures*, vol. 28, no. 8, Article ID 085028, 2019.
- [6] Y. Zhu, X. Yang, T. Fu, X. L. Yang, and T. T. Fu, "Dynamic modeling and experimental investigations of a magnetostrictive nozzle-flapper servovalve pilot stage," *Proceedings of the Institution of Mechanical Engineers - Part I: Journal of Systems & Control Engineering*, vol. 230, no. 3, pp. 244–254, 2016.
- [7] S. Y. Cao, B. W. Wang, J. J. Zheng, and W. Yan, "Hysteresis compensation for giant magnetostrictive actuators using dynamic recurrent neural network," *IEEE Transactions on Magnetics*, vol. 42, no. 4, pp. 1143–1146, 2006.
- [8] N. N. Sarawate and M. J. Dapino, "A dynamic actuation model for magnetostrictive materials," *Smart Materials and Structures*, vol. 17, no. 6, Article ID 065013, 2008.

- [9] Y. S. Li, Y. Zhu, H. Wu, D. Tang, and H. T. Wu, "Modeling and inverse compensation for giant magnetostrictive transducer applied in smart material electrohydrostatic actuator," *Journal of Intelligent Material Systems and Structures*, vol. 25, no. 3, pp. 378–388, 2014.
- [10] R. Szweczyk, "Unified first order inertial element based model of magnetostrictive hysteresis and lift-off phenomenon," *Materials*, vol. 12, no. 10, p. 1689, 2019.
- [11] G. Engdahl, *Handbook of Giant Magnetostrictive Materials*, CRC Press, San Diego, CA, USA, 2000.
- [12] W. Li, W. Fu, and W. N. Fu, "Finite element method of nonlinear magnetic field computation embedded with different vector Jiles-Atherton hysteresis models," *International Journal of Applied Electromagnetics and Mechanics*, vol. 55, pp. 135–140, 2017.
- [13] C. Tian and H. Z. Wang, "Dynamic free energy hysteresis model in magnetostrictive actuators," *Chinese Journal of Mechanical Engineering*, vol. 19, no. 1, pp. 85–88, 2006.
- [14] X. Tan and J. S. Baras, "Modeling and control of hysteresis in magnetostrictive actuators," *Automatica*, vol. 40, no. 9, pp. 1469–1480, 2004.
- [15] Y. Bin-tang, Z. Yin, P. Zhi-ke, M. Guang, and Z. K. Peng, "Real-time compensation control of hysteresis based on Prandtl-Ishlinskii operator for GMA," *Optics and Precision Engineering*, vol. 21, no. 1, pp. 124–130, 2013.
- [16] X. J. Zheng, L. Sun, and k. Jin, "A dynamic hysteresis constitutive relation for giant magnetostrictive materials," *Mechanics of Advanced Materials and Structures*, vol. 16, pp. 516–521, 2009.
- [17] Y. W. Park and M. D. Noh, "1-D and 2-D magnetostrictive actuators," *IEEE Transactions on Magnetics*, vol. 55, no. 7, pp. 1–5, 2019.
- [18] V. Apicella, C. S. Clemente, D. Davino, D. Leone, and C. Visone, "Review of modeling and control of magnetostrictive actuators," *Actuators*, vol. 8, no. 2, p. 45, 2019.
- [19] Y. S. Li, Y. C. Zhu, and H. T. Wu, "Hysteresis nonlinearity model of giant magnetostrictive actuator based on least squares support vector machine," *Machine Tool and Hydraulics*, vol. 40, pp. 5–8, 2012.
- [20] Z. Zhu, F. Liu, H. Sheng, J. Xu, and H. Sheng, "Nonlinear dynamic characteristics and control of giant magnetostrictive-piezoelectric composite actuator," *International Journal of Applied Electromagnetics and Mechanics*, vol. 59, no. 1, pp. 291–298, 2019.
- [21] Y. Li, P. Zhang, Z. He et al., "A simple magnetization model for giant magnetostrictive actuator used on an electronic controlled injector," *Journal of Magnetism and Magnetic Materials*, vol. 472, pp. 59–65, 2019.
- [22] D. Stachowiak and A. Demenko, "Finite element and experimental analysis of an axisymmetric electromechanical converter with a magnetostrictive rod," *Energies*, vol. 13, no. 5, p. 1230, 2020.
- [23] L. Xu Hui, G. Lei, W. Yan, S. Haoran, H. Yong, and W. Yan, "Micro-displacement amplifier of giant magnetostrictive actuator using flexure hinges," *Journal of Magnetism and Magnetic Materials*, vol. 556, Article ID 169415, 2022.
- [24] Y. Li, W. Huang, B. Wang, L. Weng, and B. W. Wang, "High-frequency output characteristics of giant magnetostrictive transducer," *IEEE Transactions on Magnetics*, vol. 55, no. 6, pp. 1–5, 2019.
- [25] P. Li, Q. Liu, X. Zhou et al., "Effect of Terfenol-D rod structure on vibration performance of giant magnetostrictive ultrasonic transducer," *Journal of Vibration and Control*, vol. 27, no. 5-6, pp. 573–581, 2021.
- [26] B. Dai, Z. He, Z. Yang et al., "Modeling and analysis of the piezomagnetic, electromagnetic, and magnetostrictive effects in a magnetostrictive transducer," *AIP Advances*, vol. 11, no. 12, Article ID 125213, 2021.
- [27] X. L. Yang, Y. C. Zhu, and S. S. Fei, "Magnetic field analysis and optimization of giant magnetostrictive electrohydrostatic actuator," *Journal of Aerospace Power*, vol. 31, pp. 2210–2217, 2016.